WISE photometry of EXor sources and candidates

D.Lorenzetti [a,*], T.Giannini [a]

[a] *INAF - Osservatorio Astronomico di Roma - Via Frascati, 33 - 00040 Monte Porzio Catone, Italy*

Abstract

We present the *WISE* catalog of EXor sources and candidates more recently identified. This compilation is the first complete survey of such objects in the mid-IR (3.4 - 22 μm) carried out with the same instrumentation. Two color diagrams constructed with *WISE* data evidence a clear segregation between classical and newly identified sources, being these latter characterized by colder (and less evolved) circumstellar disks. By combining 2MASS and *WISE* data, spectral energy distributions (SEDs) are obtained. Their behaviour substantially confirms the results based on *WISE* colors and offers some clue on the existence of an inner hole in the circumstellar disk. A compilation of all the EXor observations given in the literature at frequencies very similar to those of *WISE* is also provided: it allows us to search for the their mid-IR variability that has been so far poorly investigated without any coordination effort with shorter wavelengths surveys. The presented *WISE* catalog together with the compilation of the literature data are intended as a first step toward the contruction of a significant database in this spectral regime. Preliminary indications on the mechanisms responsible for the fluctuations are provided.

Key words: Stars: pre-main sequence, variable, infrared: stars, Astronomical Data Bases: catalogs

1 Introduction

Two decades ago a new class of young stellar objects (YSOs) was defined and studied by Herbig (1989, 2008) who dubbed them as EXor, after the

* Corresponding author.
Email addresses: dario.lorenzetti@oa-roma.inaf.it (D.Lorenzetti), teresa.giannini@oa-roma.inaf.it (T.Giannini).

example of the first recognized, EX Lup. These pre-Main Sequence stars are characterized by repetitive outbursts in optical light that have an amplitude up to 4-5 mag. Such oubursts typically last one year or less and are superposed on long lasting (5-10 yr) quiescence periods. They are due to intermittent accretion events during which the matter accumulated in the inner parts of the circumstellar disks is violently transferred onto the central star provoking a shock on its surface, whose cooling determines an impulsive increase of its luminosity. The physical mechanism and the observational appearance of the EXor events are substantially similar to the FUor ones (Hartmann & Kenyon 1985), although these latter present outbursts of larger intensity and remain in that state for longer period (tens of years).

So far, about 20 EXor systems are known which can be grouped into two subclasses: the classical EXor (Herbig 1989, 2008), and the newest identifications (listed in Lorenzetti et al. 2012); in that paper similarities and differences between both classes are discussed in deep detail, here we recall that the newest ones are in general more embedded objects whose phenomenology is typically observed at infrared (IR) (1-10 μm) wavelengths. Indeed, given the mechanism that originates the outburst, there is no reason which prevents the intermittent accretion to occur also during a more embedded phase. To infer on the modalities of EXor fluctuations, we are conducting since some years a photometric (Lorenzetti et al. 2007) and spectroscopic (Lorenzetti et al. 2009, 2012b) monitoring of EXor in the near-IR. Of particular interest is the mid-IR domain (3-25 μm) where many EXor emit most of their energy. The spectral behaviour at these wavelengths is strictly related to disk and envelope regions located at radial distances from the central star where disk fragmentation and planet formation occur. The difficult access to facilities operating in this spectral range has hampered this kind of studies, apart few important exceptions (Kospal et al. 2012 and references therein). However, during the last years IR surveys (eg. *MSX, Spitzer, AKARI*) allowed the investigation of entire samples of sources at mid-IR frequencies. Very recently, the satellite *WISE* (Wright et al. 2010) has covered the whole sky at 3.4, 4.6, 12, and 22 μm, and we present here the *WISE* photometry of the EXor aiming at: (*i*) building up the first mid-IR catalog of these objects that would serve as a reference for the future (hopefully increasing) and the past (unfortunately very few and sparse) observations; (*ii*) providing a complete database for constructing spectral energy distributions and affording their analysis: (*iii*) fostering the study of the EXor variability in this still unexplored spectral range, practically unaffected by extinction. The paper is organized in the following way: in Sect.2 we introduce the investigated EXor providing their *WISE* photometry that is discussed in Sect.3. In Sect.4 a database of the mid-IR observations collected so far in photometric bandpasses very similar to those of *WISE* is given along with a short discussion on the detected variability cases. Finally, our concluding remarks are presented in Sect.5.

2 Our sample and *WISE* catalog

The sample we consider in the present paper is composed by the classical and newest EXor that are listed in the upper and lower part of Table 1, respectively. Physical parameters of all these objects (with the corresponding references) can be found in Table 1 of Lorenzetti et al. 2012a. In the present Table 1 the *WISE* catalog of EXor is given (columns 2 to 9) in term of magnitudes and relative errors. As described by Cutri et al. 2012, all magnitudes listed in the WISE Source Catalog have been photometrically calibrated using observations of a network of standard stars that are located near the ecliptic polar caps; in that paper is also described the process by which instrumental source magnitudes were converted to calibrated magnitudes. All the sources listed in Table 1 present a photometric quality flag AAAA, which means that the source is detected in all 4 bands with a signal-to-noise ratio > 10. As additional information, in columns 10 and 11 of Table 1 are given: the distance (in arcsec) separating the positions of the *WISE* source and associated 2MASS PSC source and Position Angle (in degrees from N to E) of the vector from the sources. In the large majority of cases (14 out of 18) such distance is $\lesssim 1$ arcsec, that proves 2MASS and *WISE* are almost certainly looking at the same source.

We notice that two sources, namely PV Cep and GM Cep, will not be considered in our following analysis because their membership to the EXor class is highly questionable: PV Cep is now considered as Herbig Ae star, or a massive and luminous object (Kun et al. 2011a; Lorenzetti et al. 2011); GM Cep could be characterized by recurrent fadings instead of outbursts (Sicilia-Aguilar et al. 2008; Xiao et al. 2010).

3 Results and discussion on the catalog

3.1 WISE color diagrams

The *WISE* catalog given in Table 1 is presented in Figure 1 in form of two color plots [3.4-4.6] (lower panel) vs. [4.6-12] and [4.6-12] vs. [12-22] (upper panel). The EXor are located in loci framed by a color dispersion $\gtrsim 2$ mag: between 0.4 and 3 mag for the color [3.4-4.6] and between 1 and 3 mag for all the other colors. Expectedly, these are the loci typically pertaining to the pre-Main Sequence objects characterized by a significant level of IR excess over the photospheric continuum. Classical (newest) EXor are represented

in Figure 1 with blue open (red solid) symbols, respectively; a segregation between the two sub-classes is noticeable in all the colors, being the newest also the reddest objects. Particularly evident is the segregation in the color [3.4-4.6], which is $>$ ($<$) than 1 for the newest and classical EXor, respectively (the unity value corresponds to a ratio $F_\nu(3.4\mu m)/F_\nu(4.6\mu m) \approx 4$). Classical objects are certainly less extincted than the newest ones, hence the extinction has definitely a role in determining the color separation noticeable in the *WISE* plots, however, it is not the sole responsible for that. Indeed, the arrow depicted in the lower panel of Figure 1 indicates the de-reddening effect that corresponds to an $A_V = 10$ mag, and, even allowing for larger A_V values, newest EXor can be never superposed to the classical ones. The SEDs of the former should be intrinsically different, namely characterized by a larger emission from dust mainly at lower temperatures (see below). From Figure 1 is also evident that the *WISE* colors of EXor are not consistent with a single balckbody, but can be described in terms of different dust components with the warmest temperature ranging between 1000 and 3000 K and the lowest one between 380 and 500 K. Oversimplifying, only couples of blackbody are depicted in Figure 1, but a more realistic stratification of temperatures should be envisaged.

3.2 EXor near- and mid-IR SEDs

We obtained the near- and mid-IR SEDs of EXor by identifying the counterparts at shorter wavelengths (JHK bands) of the sources listed in our *WISE* catalog (Table 1). Unfortunately, a single epoch SED cannot be constructed since coordinated observations in different spectral ranges are very rare (see Sect. 4). However, to rely on a data-base as uniform as possible,, we considered the 2MASS (Cutri et al 2003) counterparts that match our sources within 2 arcsec or less (see Table 1). All the catalogued EXor (except one, V2492 Cyg) have been associated to a 2MASS counterpart and the resulting SEDs are depicted in Figures 2 and 3. For comparison, a median stellar photosphere in the spectral range K5-M5 is also plotted in each panel (Hernández et al. 2007), normalized to the J band flux of any single source. As anticipated by the two color diagrams, also the SED shapes of the two sub-classes are substantially different. All the classical EXor (except NY Ori) decline by increasing the wavelength for $\lambda \lesssim 10$ μm; at $\lambda \gtrsim 10$ μm their SEDs tend to increase, showing an excess more pronounced than that at shorter wavelengths. Conversely, the newest candidates (apart two exceptions) have SEDs that monotonically increase with the wavelength. The spectral distributions of both classes are fully consistent with those predicted by D'Alessio et al. (1999), namely they are originated by a temperature stratification due to a more (classical EXor) or less (newest ones) evolved circumstellar disk. To define more quantitatively the EXor SEDs, we introduce, as empirical indicator, the parameter ε, ie. the

ratio between the observed SED and the underlying median K5-M5 photosphere, both integrated from J to 22 μm. The resulting values are given in the last column of Table 1: the relatively modest excess presented by the classical EXor is accounted for by their ε values $\lesssim 20$, while the newest ones present ε typically $\gg 200$, except the two unobscured T Tauri stars V2492 and V2493 Cyg. This short analysis evidences how the mid-IR emission is crucial for observationally defining the EXor class of objects. Finally, and more speculatively, we can observe that the majority of the EXor' SEDs (10 out of the 16 depicted in Figures 2 and 3) seems to show a deficit of emission around 3 μm. This apperance should be considered very cautionsly since that wavelength is exactly the matching point between 2MASS and *WISE* photometry, and 2MASS data were obtained about ten years prior to the *WISE* advent. On the other hand, a systematic trend according to which *WISE* data would have been taken when all the sources were in stage more quiescent than 2MASS, sounds remarkably strange. However, if such an emission deficit will be confirmed by forthcoming observations, it reasonably indicates a lack of emission in that spectral range, which is usually interpreted in terms of circumstellar disk with an inner hole, a scenario which is largely supported by both photometric (Sipos et al. 2009, Lorenzetti et al 2012) and mainly interferometric (Akeson et al. 2005, Eisner et al. 2010) studies.

4 Mid-IR variability

To ascertain if EXor present significant fluctuations in the *WISE* mid-IR range as they certainly do in the optical/near-IR, we have collected in Tables 2 and 3 the observations carried out in the bands L ($\sim$3μm), M ($\sim$5μm), N ($\sim$10μm), and Q ($\sim$20μm), presented so far in the literature. To construct these Tables we have adopted the following data: all the ground-based observations, IRAS 12 and 25 μm, MSX 12 and 21 μm, *Spitzer* IRAC 3.4 and 4.5 μm, and *Spitzer* MIPS 24 μm. Data taken in different, although adjacent, bands (eg. IRAC 5.8 and 8.0 μm) have not been considered because of the larger difference between their and *WISE* bandpasses. The epoch of any single observation and the effective wavelength of the used bandpass are also given in Tables 2 and 3. For an easier comparison, the values corresponding to the L, M (N, Q) bands are given in magnitudes (in Jansky): in some cases, the photometric values found in the literature have been converted into magnitude or fluxes by adopting the zero-magnitude fluxes given in the WEB resources of the Gemini Observatory (http://www.gemini.edu/?q=node/11119), whenever the conversion values are not given in the original paper. This procedure, together with the comparison between bandpasses which are not perfectly coincident, is affected by instrumental and calibration effects and may cause a scatter up to 50%. This scatter is larger than the errors of any single measurement, never-

theless it has to be considered as the real uncertainty. Hence, fluctuations up to that amplitude have be considered as negligible for the present work, unless they have been detected with the same instrumentation: these cases will be mentioned below. IRAS fluxes are listed just for completeness, but not considered for the quantitative comparison, because they are taken with a beam size much larger than that of other observations. Data in Tables 2 and 3, complemented with *WISE* observations are summarized in a more readable form in Figure 4: here the histogram of sources as a function of the amplitude of their fluctuations in the two most illustrative L and N bands is given for both classical (dashed black line) and newest (solid red line) EXor; Δmag values correspond to (L_{max} - L_{min}) and 2.5·Log[F_{max}(N)/F_{min}(N)], respectively.
As mentioned before, the fluctuations corresponding to the first bin are neglected; larger values (up to Δmag 3-5) mainly occur in the newest objects: this fact is due in part to their intrinsically different nature (ie. dominated by colder dust), but it is also a bias effect related to the larger number of mid-IR observations available for the newest sources. The amplitude of these fluctuations is comparable with that occurring in the near-IR, where a decreasing trend with the increasing wavelength was noted (Lorenzetti et al. 2007). In other words, it seems that from $\lambda >$ 2- 3 μm the amplitude of the fluctuations becomes independent on λ. This likely means that the Δmag decreasing trend in the optical and near-IR bands is essentially related only to the stellar component, while in the frequency regime where dust emission starts to dominate, any spectral trend is not so evident.

4.1 Variability timescales

The timescale of the mid-IR variability is even more important than the variability itself, since it can elucidate on the physical mechanism responsible for the fluctuations. The previous analysis is typically based on timescales of years or even longer, while only investigations at shorter timescales can effectively constrain the working physical mechanism(s). To that scope, it is worthwhile to dig out the Tables 2 and 3 for extracting those monitoring observations executed on shorter timescales and with the same instrumentation so to avoid any inter-calibration uncertainty. These cases are summarized in Table 4: here we list the epoch and the spectral band of the monitoring (cols.2 and 3), its timescale (col.4), and the largest Δmag detected (col.5), compared with the 1σ error (col.6). We define as significant those sampling for which Δmag $> 3\sigma$ and marked them in boldface. All the sources daily sampled in the L band (namely DR Tau, V1180 Cas, and V512 Per) show $\sim$ 0.3 mag variations on that timescale; DR Tau presents significant variations even on hour timescale. These very short timescales can be related to the response time of the dust particles to the energy input provoked by the accretion event or to fast changes of the dust distributions (Kun et al. 2011). Basing upon a still rather poor

statistics (3 positive cases out of 3 investigated), we can tentatively conclude that all EXor are affected by variations of the same amplitude (0.3 mag) on the same timescale (days): if this were the case, the response of the dust particle should be preferred to the dust re-arrangements, since the constancy of the observables seems more compatible with an intrinsic property of the dust grains, more than with a changing dust morphology that should unexpectedly follow the same modalities. However, to ascertain the role of both possible mechanisms, (quasi-)simultaneous ground-based observations in the near- and mid-IR (L, M bands) should be in order.

5 Concluding remarks

We have compiled the first *WISE* catalog (3.4 - 22 μm) of the mid-IR emission of both classical EXor and related objects. Analyzing the presented data the following can be summarized:

- The *WISE* catalog along with the compilation of all the mid-observations retrived from the literature represents the first step for costructing a mid-IR database of the EXor continuum emission
- In the *WISE* two color plots the classical and the newly defined EXor are distinguishable since the latter present a more prominent emission by their circumstellar disks that appears also colder and less evolved.
- EXor's SED confirm the previous result giving also argument in favour of an inner hole in the circumstellar disk, as predicted by theory and observed by interferometric investigations.
- A search for mid-IR variability has started and the preliminary results indicate that (*i*) the amplitude of the fluctuations is comparable to that occurring in near-IR without any decreasing trend with wavelength; and (*ii*) all the sources sampled on a daily timescale presents significant variations. Implications on possible mechanisms have been discussed.

References

- Ábrahám, P., Kóspál, Á., Csizmadia, Sz., Moór, A., Kun,M., & Strigfellow, G. 2004, A&A, 419, L39
- Akeson, R.L. et al. 2005, ApJ, 622, 440
- Aspin, C. 2011a, AJ, 141, 196
- Aspin, C. 2011b, AJ, 142, 135
- Aspin, C. et al. 2009, ApJ, 692, L67
- Aspin, C., Beck, T.L., & Reipurth, B., G. 2008, AJ, 135, L35
- Aspin, C. & Sandell, G. 1994, A&A, 288, 803
- Aspin, C. & Sandell, G. 1997, MNRAS, 289, 1
- Appenzeller, I., Jankovics, I. & Krautter, J. 1983, A&A 53, 291
- Breger, M., Gehrz, R.D. & Hackwell, J.A. 1981, ApJ 248, 963
- Chen, X., Launhardt, R. & Henning, T. 2009, ApJ 691, 1729
- Cohen, M. 1974, MNRAS, 169, 257
- Cohen, M. & Kuhi, L. 1979, ApJS, 41, 743
- Cohen, M. & Schwartz, R.,D. 1983, ApJ, 265, 887
- Cutri, R.M. et al. 2003, Explanatory Supplement to the 2MASS All Sky Data Release (Pasadena, CA:Caltech)
- Cutri, R.M. et al. 2012, http://wise2.ipac.caltech.edu/docs/release/allsky/expsup/
- D'Alessio, P., Calvet, N., Hartmann, L., Lizano, S. & Cantó, J. 1999, ApJ 527, 893
- Eisner, J.A. et al. 2005, ApJ, 718, 774
- Elias, J.H. 1978, ApJ, 224, 857
- Fischer, W.J. et al. 2012, arXiv:1207.2466v1
- Ghez, A.M., Emerson, J.P., Graham, J.M., Meixner, M. & Skinner, C.J. 1994, ApJ, 434, 707
- Glass, I.S. & Penston, M.V. 1974, MNRAS 167, 237
- Guieu, S. et al. 2009, ApJ, 697, 787
- Hartmann, L. et al. 2005, ApJ, 629, 881
- Hartmann, L., & Kenyon, S. 1985, ApJ, 299, 462
- Herbig, G.H. 1989, Proc. of the ESO Workshop on *Low Mass Star Formation and Pre-Main Sequence Objects*, ed. B. Reipurth, p.233
- Herbig, G.H. 2008, AJ, 135, 637
- Hernández, J. et al. 2007, 662, 1067
- Hodapp, K.-W., Hora, J.L., Rayner, J.T., Pickles,& Ladd, E.F. 1996, ApJ, 468, 861
- Hughes, J., Hartigan, P., Krautter, J., & Kelemen, J. 1994, AJ, 108, 1071
- Kenyon, S.J. et al. 1994, AJ, 107, 2153
- Kenyon, S.J. & Gómez, M. 2001, AJ, 121, 2673

  Kóspál, Á., Ábrahám, P., Prusti, T., acosta-Pulido, J., Hony, S., Moór, A., & Siebenmorgen, R. 2007, A&A, 470, 211

  Kóspál, Á. et al. 2012, ApJS, 201, 11
- Kun, M. et al. 2011a, MNRAS, 413, 2689
- Kun, M. et al. 2011b, ApJ, 733, L8

- Liseau, R., Lorenzetti, D., & Molinari, S. 1992, A&A, 253, 119
- Lorenzetti, D. et al. 2011, ApJ, 732:69
- Lorenzetti, D. et al. 2012a, ApJ, 749:188
- Lorenzetti, D. et al. 2012b, New Astronomy, submitted
- Lorenzetti, D., Giannini, T., Larionov, V.M., Kopatskaya, E., Arkharov, A.A., De Luca, M., & Di Paola, A. 2007, ApJ, 665, 1182
- Lorenzetti, D., Larionov, V.M., Giannini, T., Arkharov, A.A., Antoniucci, S., Nisini, B., & Di Paola, A. 2009, ApJ, 693, 1056
- McCabe, C., Ghez, A.M., Prato, L., Duchêne, G., Fisher, R.S., & Telesco, C. 2006, ApJ, 636, 932
- Muzerolle, J., Megeath, S.T., Flaherty, K.M., Gordon, K.D., Rieke, G.H., Young, E.T., & Lada, C.J. 2005, ApJ, 620, L107
- Persi, P., Tapia, M., Gòmez, M., Whitney, B.A., Marenzi, A.M., & Roth, M. 2007, AJ, 133, 1690
- Przygodda, F., van Boekel, R., Ábrahám, P. et al. 2003, A&A 412, L43
- Rebull, L.M., Stauffer, J.R., Megeath, S.T., Hora, J.L., & Hartmann, L. 2006, ApJ, 646, 297
- Rieke, G.H., & Lebofsky, M.J. 1984, ApJ, 288, 618
- Rydgren, A.E. 1984, Publ. USNO, 25, 1
- Rydgren, A.E., Strom, S.E., & Strom, K.M. 1976, ApJS, 30, 307
- Rydgren, A.E. & Vrba, F.J. 1983, AJ 88, 1017
- Sicilia-Aguilar, A. et al. 2008, ApJ, 673, 382
- Sipos, N. et al. 2009, A&A, 507, 881
- Stecklum, B., Melnikov, S.Y., & Meusinger, H. 2007, A&A, 175, 231
- Thi, W.F. et al. 2001, ApJ, 561, 1074
- Weaver, W.B. & Jones, G. 1992, ApJS 78, 239
- Wright, E.L. et al. 2010, AJ, 140, 1868
- Xiao, L., Kroll, P., & Henden, A.A. 2010, AJ, 139, 1527

Table 1
WISE photometry of Exor and related objects.

Source	3.4μm	err 1	4.6μm	err 2	12μm	err 3	22μm	err 4	(2MASS)		ε
				(mag)					D (")	PA (deg)	
UZ Tau E	6.34	0.04	5.72	0.02	3.67	0.01	1.78	0.01	0.3	223.8	5.8
VY Tau	8.48	0.02	8.03	0.02	6.22	0.02	4.73	0.03	0.1	150.3	1.7
DR Tau	5.68	0.06	4.67	0.04	2.99	0.01	1.04	0.02	0.1	81.0	8.9
V1118 Ori	9.85	0.02	9.01	0.02	6.92	0.10	3.48	0.05	0.1	150.3	9.7
NY Ori	6.87	0.03	6.27	0.02	3.30	0.02	0.93	0.03	0.4	275.0	21.6
V1143 Ori	11.37	0.02	10.90	0.02	8.68	0.03	6.40	0.06	0.2	111.0	1.8
EX Lup	8.19	0.02	7.63	0.02	4.50	0.01	2.33	0.02	0.2	195.9	3.5
PV Cep[a]	5.26	0.07	3.31	0.07	0.76	0.01	-1.22	0.01	1.9	265.0	—
V1180 Cas	9.56	0.02	8.29	0.02	5.56	0.01	3.61	0.04	0.18	258.4	534
V512 Per	6.75	0.03	4.89	0.03	1.44	0.01	-1.69	0.01	0.28	116.1	212
LDN1415 IRS	10.71	0.02	8.94	0.02	4.94	0.01	1.46	0.01	4.6	5.8	1041
V2775 Ori	6.78	0.03	5.41	0.03	3.03	0.01	0.75	0.01	0.10	23.2	5951
V1647 Ori	6.26	0.05	4.85	0.03	1.90	0.01	-0.48	0.01	0.10	241.6	3233
GM Cha	10.07	0.03	7.79	0.02	4.24	0.01	0.91	0.01	0.30	40.8	1706
OO Ser	11.83	0.03	8.94	0.02	4.47	0.01	0.59	0.01	0.70	192.0	$>1.3\ 10^4$
V2492 Cyg	5.90	0.05	4.32	0.03	2.01	0.01	0.09	0.01	—	—	5.5
V2493 Cyg	9.50	0.02	8.47	0.02	6.70	0.02	4.75	0.05	2.53	196.0	14.9
GM Cep[a]	7.47	0.03	6.81	0.02	4.42	0.01	2.56	0.02	1.05	170.7	—

- The fluxes corresponding to zero magnitude are: 309.5 Jy, 171.8 Jy, 31.67 Jy, and 8.363 Jy for the bands at 3.4, 4.6, 12, and 22, respectively (Cutri et al. 2012).
- The quality flag is AAAA for all the sources.
[a] Its membership to the EXor class is widely debated (see text).

Table 2
L and M band photometry of EXor.

Source	Epoch	L band		M band	
		(mag)	[λ_{eff}] - Ref	(mag)	[λ_{eff}] - Ref
UZ Tau E	73/74	6.2 ± 0.2	[3.6] - 1		
	Nov 76	6.29	[3.4] - 2		
	Dec 76	6.4 ± 0.1	[3.4] - 2	5.6 ± 0.3	[4.8] - 2
	Nov 77	6.04 ± 0.02	[3.5] - 3		
	Jan 81	6.29	[3.4] - 4	5.55	[4.8] - 4
	Dec 01[a]	6.42 ± 0.17	[3.5] - 5		
	Mar 04	5.98 ± 0.03	IRAC[3.4] - 6	5.46 ± 0.04	IRAC[4.5] - 6
VY Tau	73/74	8.6 ± 0.2	[3.6] - 1		
	Dec 73	8.3 ± 0.1	[3.5] - 7		
	Nov 77	8.9 ± 0.1	[3.5] - 3		
	Dec 81	8.50 ± 0.06	[3.5] - 8		
	Dec 01	8.31 ± 0.09	[3.5] - 5		
DR Tau	72/74	5.9 ± 0.2	[3.6] - 1		
	Nov 73	5.8 ± 0.05	[3.5] - 7	5.0 ± 0.2	[4.8] - 7
	Nov 77	4.83± 0.05	[3.5] - 3		
	Dec 81	5.34± 0.04	[3.5] - 8		
	Dec 81	5.15± 0.04	[3.5] - 8	4.17	[xxx] - 4
	Nov 87	5.01 - 5.32	[3.8] - 9	4.47 - 4.69	[4.7] - 9
	Sep 88	4.93 - 5.46	[3.8] - 9		
	96/98	5.3[b]	[3.4] - 10		
	Mar 04			4.5	IRAC[4.5] - 6
V1118 Ori	Oct 04	9.85 ± 0.002	IRAC[3.4] - 11	9.08± 0.002	IRAC[4.5] - 11
NY Ori	Sep 75	> 9	[3.6] - 12		
V1143 Ori					
EX Lup	Jun 73	> 8.7	[3.4] - 13		
	Apr 82	8.02± 0.01	[?] - 14	7.54± 0.05	[?] - 14
	Apr 82	8.05± 0.01	[3.4] - 15	7.54± 0.05	[4.8] - 15
	Feb/Sep 97	(8.0-8.2)±0.1	[3.6] - 16		
	Mar 05	7.92 ± 0.02	IRAC[3.4] - 16	7.35± 0.02	IRAC[4.5] - 16

Table 2
Continued.

Source	Epoch	L band		M band	
		(mag)	[λ_{eff}] - Ref	(mag)	[λ_{eff}] - Ref
V1180 Cas	Mar 09	9.50± 0.06	IRAC[3.4] - 17	8.58± 0.04	IRAC[4.5] - 17
	Oct/Nov 09	(8.99-9.28)±0.01	IRAC[3.4] - 17	(8.05-8.30)± 0.01	IRAC[4.5] - 17
V512 Per	< 83	6.37±0.01	[3.5] - 18	4.71±0.09	[4.6] - 18
	Sep 88	(5.20-5.59)±0.03	[3.91] - 19	> 4.2	[4.7] - 19
	Jan 89	(5.3-5.7)±0.2	[3.91] - 19	> 4.7	[4.7] - 19
	Feb 90	5.3±0.1	[3.91] - 19	> 4.4	[4.7] - 19
	Oct 90	5.28±0.02	[3.91] - 19	4.2±0.1	[4.7] - 19
	Sep 91	5.88±0.05	[3.6] - 20		
	Mar 92	6.11±0.05	[3.6] - 20		
	Nov 92	6.11±0.05	[3.42] - 20		
	Feb 93	5.96±0.05	[3.42] - 20		
	Oct 93	(6.18-6.36)±0.05	[3.42] - 20		
	Dec 93	6.48±0.05	[3.42] - 20		
	Dec 93	6.60±0.05	[3.42] - 21		
	Sep 04	7.45±0.07	IRAC[3.4] - 22	6.39±0.09	IRAC[4.5] - 22
LDN1415IRS					
V2775 Ori	Feb/Oct 04	8.46±0.05	IRAC[3.4] - 23	7.66±0.05	IRAC[4.5] - 23
V1647 Ori	Mar 04	5.33	IRAC[3.4] - 24	4.41	IRAC[4.5] - 24
	Feb 07	7.6±0.1	[3.4] - 25		
	Sep 08	5.8±0.1	[3.4] - 25		
	Feb 11	5.6±0.1	[3.4] - 25		
GM Cha	Mar 99	8.32±0.05	[3.5] - 26		
	Jul 04	8.42±0.08	IRAC[3.4] - 27	6.98±0.07	IRAC[4.5] - 27
OO Ser	Oct 95	6.9	[3.8] - 28	5.2	[4.8] - 28
	Feb 96	8.1±0.1	[3.6] - 29	5.36±0.01	[4.8] - 29
	Apr 96	8.2±0.1	[3.6] - 29	5.45±0.03	[4.8] - 29
	Sep 96	8.22±0.08	[3.6] - 29	5.84±0.04	[4.8] - 29
	Oct 96	8.9±0.4	[3.6] - 29	5.9±0.4	[4.8] - 29
	Mar 97	8.9±0.1	[3.6] - 29	6.13±0.05	[4.8] - 29
	Apr 97	9.06±0.08	[3.6] - 29	5.98±0.04	[4.8] - 29
	Sep 97			6.3±0.4	[4.8] - 29
	Apr 04	11.5±0.1	IRAC[3.4] - 29	8.35±0.02	IRAC[4.5] - 29
V2492 Cyg	Jul 06	8.94±0.09	IRAC[3.4] - 30	7.6±0.1	IRAC[4.5] - 30
	Sep 10	5.4±0.1	[3.8] - 30		
	Nov 10	6.0±0.1	[3.8] - 30		
V2493 Cyg	Nov 77	9.4±0.1	[3.5] - 3		
	Aug 06	9.9±0.1	IRAC[3.4] - 31	9.2±0.1	IRAC[4.5] - 31

- References to the Table: (1) Cohen 1974; (2) Elias 1978; (3) Cohen & Kuhi 1979; (4) Rydgren 1984; (5) McCabe 2006; (6) Hartmann et al. 2005; (7) Rydgren et al. 1976; (8) Rydgren & Vrba 1983; (9) Kenyon et al. 1994; (10) Thi et al. 2001; (11) Rebull et al. 2006; (12) Breger et al. 1981; (13) Glass & Penston 1974; (14) Appenzeller et al. 1983; (15) Hughes et al. 1994; (16) Sipos et al. 2009; (17) Kun et al. 2011a; (18) Cohen & Schwartz 1983: (19) Liseau et al. 1992; (20) Aspin & Sandell 1994; (21) Aspin & Sandell 1997; (22) Chen et al. 2009; (23) Fischer et al. 2012; (24) Muzerolle et al. 2005; (25) Aspin 2011b; (26) Kenyon & Gómez 2001; (27) Persi et al. 2007; (28) Hodapp et al. 1996; (29) Kóspál et al. 2007; (30) Aspin 2011a; (31) Guieu et al. 2009.

[a] This value refers to the total binary system, although the primary and the secondary have been resolved and separately observed.

[b] ISO-SWS continuum flux near H_2 lines.

Table 3
N and Q band photometry of EXor.

Source	Epoch	N band		Q band	
		(Jy)	[λ_{eff}] - Ref	(Jy)	[λ_{eff}] - Ref
UZ Tau E	73/74	1.6 ± 0.3	[10] - 1		
	Nov 76	1.3 ± 0.3	[10] - 2		
	Dec 76	1.0 ± 0.2	[10] - 2		
	Jan 81	1.1 ± 0.1	[10] - 3	0.8	[20] - 3
	83	1.38 ± 0.03	IRAS[12]- 4	1.76 ± 0.04	IRAS[25] - 4
	Dec 92[a]	1.06 ± 0.04	[9.5] - 5		
	Nov 99[b]	1.5 ± 0.1	[10.8] - 6	1.6 ± 0.2	[18.1] - 6
VY Tau	73/74	< 0.35	[10] - 1		
	Dec 73	0.3 ± 0.05	[10.8] - 7		
	83	0.20 ± 0.03	IRAS[12]- 4	0.29 ± 0.03	IRAS[25] - 4
	Nov 99	0.07 ± 0.01	[10.8] - 6		
DR Tau	72/74	2.2	[10] - 1		
	Nov 73	1.3	[11.1] - 7		
	83	3.16 ± 0.03	IRAS[12]- 4	4.30 ± 0.05	IRAS[25] - 4
	96/98	2.4[c]	[9.6] - 8		
	Dec 81	3.8	[10] - 3	2.9	[20] - 3
	Dec 82	2.9	[10] - 3		
	96/98	2.4[c]	[9.6] - 9		
	Dec 02	2.0	[11.9] - 10		
V1118 Ori	Jan 02	< 0.5	MSX[12] - 11		
	Jan 06	0.07 ± 0.01	[10.4] - 11		
NY Ori	83	10 ± 3	IRAS[12]- 4		
V1143 Ori	83	0.17 ± 0.04	IRAS[12]- 4	0.10 ± 0.06	IRAS[25] - 4
EX Lup	83	0.80 ± 0.03	IRAS[12]- 4	1.09 ± 0.03	IRAS[25] - 4
	Feb/Sep 97	(0.7-0.8)±0.1	ISOPHOT[12]- 12	(0.9-1.3)±0.2	ISOPHOT[20] - 12

Table 3
Continued.

Source	Epoch	N band		Q band	
		(Jy)	$[\lambda_{eff}]$ - Ref	(Jy)	$[\lambda_{eff}]$ - Ref
V1180 Cas	83	< 0.25	IRAS[12]- 13	0.72 FQUAL 3	IRAS[25] - 13
V512 Per	< 83	6.54±0.07	[10.2] - 14	25±1	[19] - 14
	83	11.2 FQUAL3	IRAS[12] - 13	42.8 FQUAL 3	IRAS[25] - 13
	Sep 04			> 21 (satur.)	MIPS[24] - 15
LDN1415IRS	83	0.15±0.05	IRAS[12]- 16	0.49±0.06	IRAS[25] - 16
V2775 Ori	Apr 05			0.68±0.03	MIPS[24] - 17
	Nov 08			5.0±0.2	MIPS[24] - 17
V1647 Ori	83	0.52	IRAS[12]- 18	1.2	IRAS[25] - 18
	Mar 04	7±1	[11.2] - 19	15.6	MIPS[24] - 20
	Mar 07	0.23	[11.2] - 21	0.44	[18.3] - 21
	Sep 08	2.8±0.5	[11.2] - 19	7±1	[18.3] - 19
GM Cha	Apr 04	1.15±0.09	[12.9] - 22		
OO Ser	Oct 95	6.4	[11.7] - 23	12.5	[20.6] - 23
	Feb 96	4±1	[12] - 24	29±3	[25] - 24
	Apr 96	4.1±0.1	[12] - 24	39±1	[25] - 24
	Sep 96	3±1	[12] - 24		
	Oct 96	4±1	[12] - 24	21±2	[25] - 24
	Mar 97	2.98±0.06	[12] - 24	18±2	[25] - 24
	Apr 97	3±1	[12] - 24	19±2	[25] - 24
	Sep 97	2.0±0.8	[12] - 24	17±2	[25] - 24
	Apr 04			13±2	MIPS[24] - 24
	Oct 04	0.6±0.1	[10.4] - 24		
V2492 Cyg	83	3.4±0.3	IRAS[12] - 25	6.6±0.6	IRAS[25] - 25
	Jul 96	2.5±0.1	MSX[12.13] - 25	3.1±0.2	MSX[21.4] - 25
	Jul 06			3.4±0.3	MIPS[24] - 25
V2493 Cyg					

- References to the Table: (1) Cohen 1974; (2) Elias 1978; (3) Rydgren et al. 1984; (4) Weaver & Jones 1992 (5) Ghez et al. 1994; (6) McCabe 2006; (7) Rydgren et al. 1976; (8) Thi et al. 2001; (9) Thi et al. 2001; (10) Przygodda et al. 2003; (11) Lorenzetti et al. 2007; (12) Sipos et al. 2009; (13) IRAS Point Source Catalog; (14) Cohen & Schwartz 1983; (15) Chen et al. 2009; (16) Stecklum et al 2007; (17) Fischer et al. 2012; (18) Ábrahám et al. 2004; (19) Aspin et al. 2009; (20) Muzerolle et al. 2005; (21) Aspin et al. 2008; (22) Persi et al. 2007; (23) Hodapp et al. 1996; (24) Kóspál et al. 2007; (25) Aspin 2011a;

[a] Spectrophotometry of the resolved component UZ Tau E in the 8-13 μm window: observations at closeby wavelengths are also available.

[b] These values refer to the total binary system, although the primary and the secondary have been resolved and separately observed.

[c] ISO-SWS continuum flux near H_2 lines.

Table 4
Systematic mid-IR monitoring cases of some EXor.

Source	Epoch	Band	timescale	Δmag	error
				(mag)	
DR Tau	**Nov 87**	**L**	**days**	**0.3**	**< 0.01**
	Sep 88	**L**	**hours**	**0.04**	**< 0.01**
EX Lup	97	L	months	0.2	0.1
V1180 Cas	**Oct/Nov 09**	**L**	**days**	**0.3**	**0.01**
	Oct/Nov 09	**M**	**days**	**0.3**	**0.01**
V512 Per	**Sep 88**	**L**	**days**	**0.4**	**0.03**
	Oct 93	**L**	**days**	**0.2**	**0.05**
OO Ser	**96/97**	**L**	**months**	**0.9**	**0.1**
	96/97	N	months	0.7	0.3

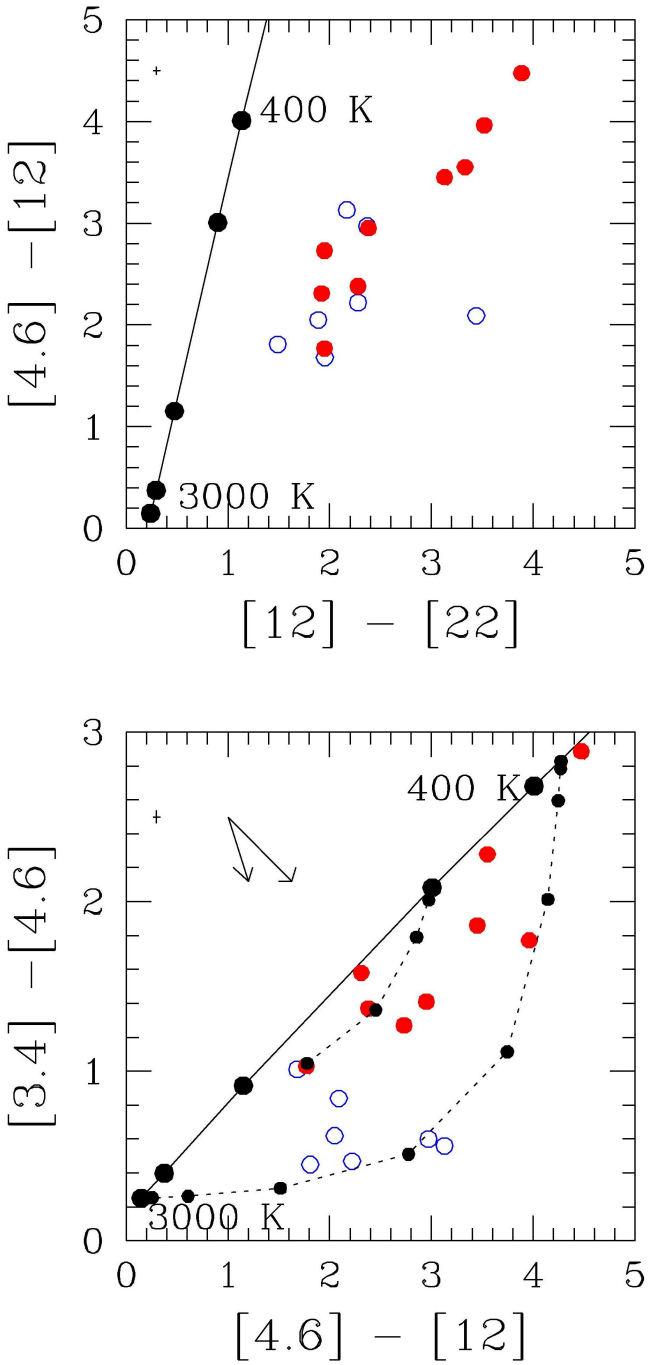

Fig. 1. *WISE* two color diagrams of EXor. The colors of the classical (newest) EXor are depicted with blue (red) open (solid) symbols. The black-body colors (at different temperatures) correspond to the black straight line. Black dashed lines in the lower panel indicate the colors of the sum of two black-bodies, where the surface of coldest one (380-500 K) is progressively increased with respect to the warmest (1000-3000 K). The reddening vectors (whose amplitude corresponds to an extinction $A_V = 10$ mag) are relative to two different values of A_λ, at 10.5 and 12.0 μm, respectively (Rieke & Lebofsky 1985). A cross in the upper left corners of both panels indicates the typical error.

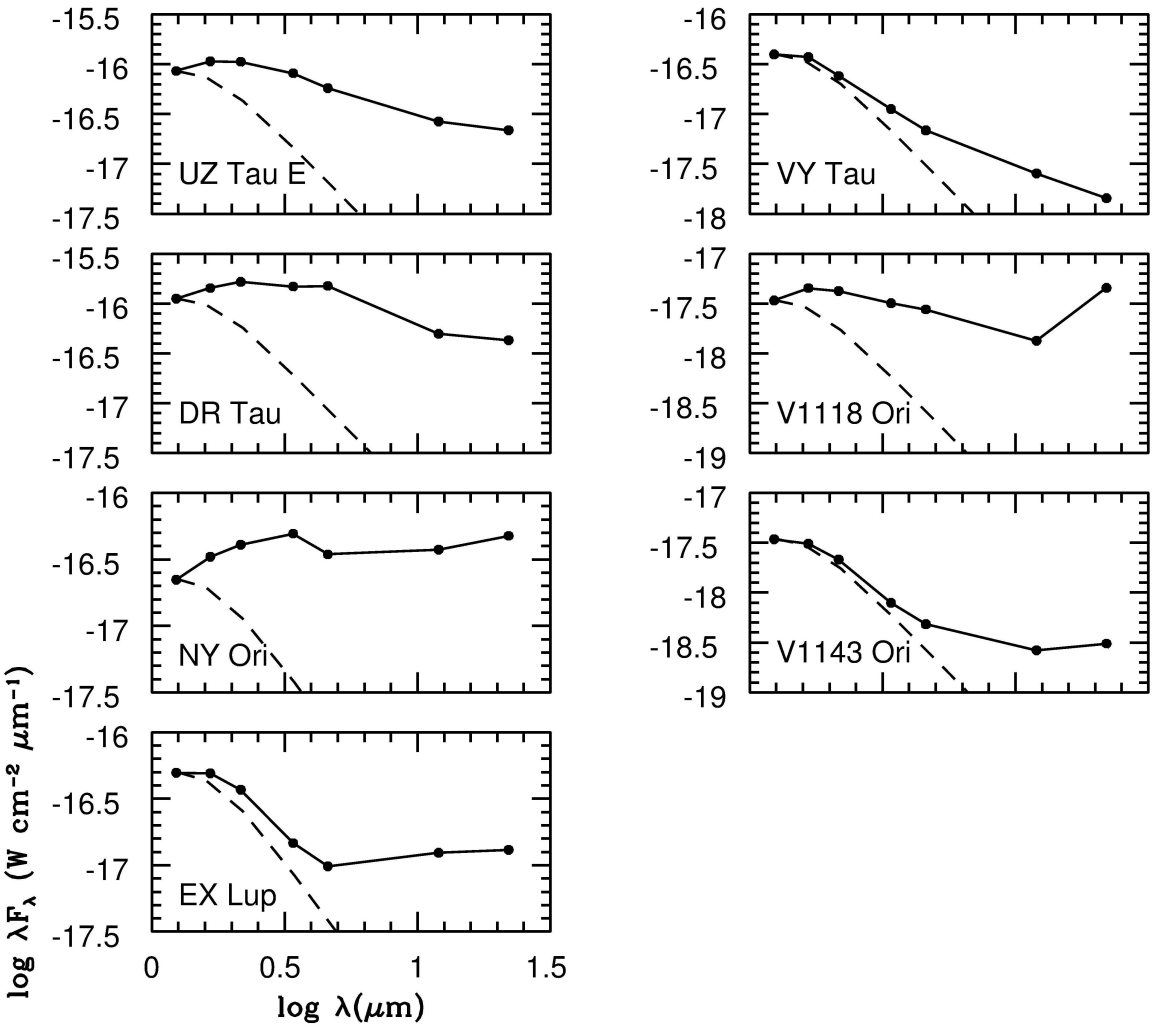

Fig. 2. EXor' SEDs in the range 1.25-22 μm of the *classical* sources composed by 2MASS and *WISE* fluxes. Dashed line represents a median photosphere of stars in the spectral range K5-M5 and normalized to the J band flux of each source.

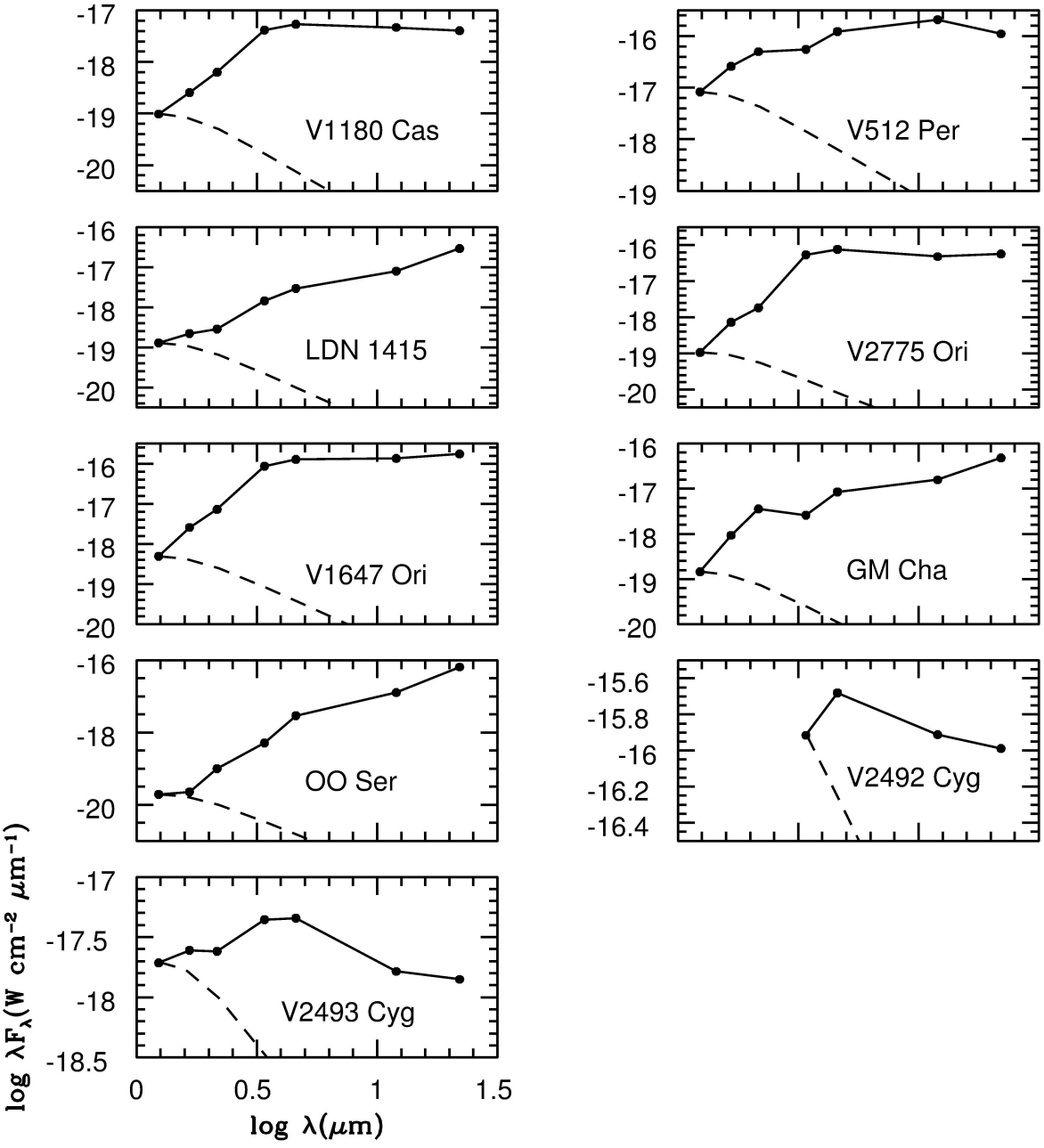

Fig. 3. Same as Figure 2 for the *newest* sources.

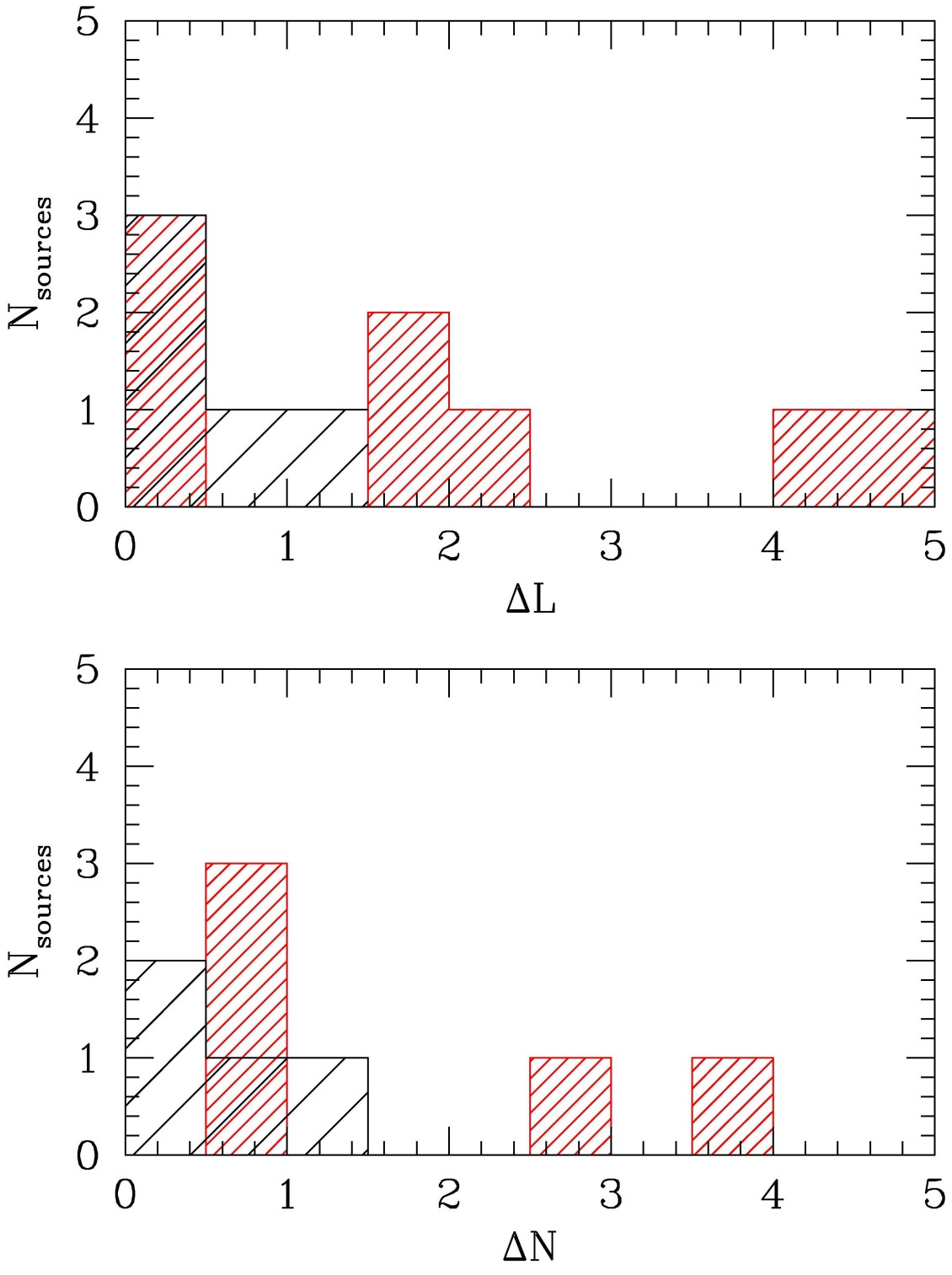

Fig. 4. Distribution of the EXor fluctuations detected in the L and N bands (see Tables 2 and 3).